Self-image Effects in Diffraction and Dispersion

H.C. Rosu[1], J. P. Treviño[1], H. Cabrera[1], and J. S. Murguía[2]

[1]*IPICyT - Instituto Potosino de Investigación Científica y Tecnológica,*
Apdo Postal 3-74 Tangamanga, 78231 San Luis Potosí, México.

[2] *Universidad Autónoma de San Luis Potosí, 87545 San Luis Potosí, SLP. México.*
emails: hcr, jpablo, cabrera@ipicyt.edu.mx, ondeleto@uaslp.mx

Talbot's self-imaging effect occurrs in near-field diffraction. In the rational paraxial approximation, the Talbot images are formed at distances $z = p/q$, where p and q are coprimes, and are superpositions of q equally spaced images of the original binary transmission (Ronchi) grating. This interpretation offers the possibility to express the Talbot effect through Gauss sums. Here, we pay attention to the Talbot effect in the case of dispersion in optical fibers presenting our considerations based on the close relationships of the mathematical representations of diffraction and dispersion. Although dispersion deals with continuous functions, such as gaussian and supergaussian pulses, whereas in diffraction one frequently deals with discontinuous functions, the mathematical correspondence enables one to characterize the Talbot effect in the two cases with minor differences. In addition, we apply the wavelet transform to the fractal Talbot effect in both diffraction and fiber dispersion. In the first case, the self similar character of the transverse paraxial field at irrational multiples of the Talbot distance is confirmed, whereas in the second case it is shown that the field is not self similar for supergaussian pulses. Finally, a high-precision measurement of irrational distances employing the fractal index determined with the wavelet transform is pointed out.

1 Introduction

Near field diffraction can produce images of periodic structures such as gratings without any other means. This is known since 1836 when this self-imaging phenomenon has been discovered by H.F. Talbot, one of the inventor pioneers of photography [1]. Take for example a periodic object as simple as a Ronchi grating which is a set of black lines and equal clear spaces on a plate repeating with period a. In monochromatic light of wavelength λ one can reproduce its image at a "focal" distance known as the Talbot distance given by $z_{\mathrm{T}} = a^2\lambda^{-1}$, a formula first derived by Lord Rayleigh in 1881 [2]. Moreover, more images show up at integer multiples of the Talbot distance. It was only in 1989 that

the first and only one review on the Talbot effect has been written by Patorski [3].

In the framework of Helmholtz equation approach to the physical optics of a δ-comb grating, Berry and Klein [4] showed in 1996 that in rational Talbot planes, i.e., planes situated at rational distances in units of the Talbot distance, the paraxial diffraction wavefield has a highly interesting arithmetic structure related to Gauss sums and other fundamental relationships in number theory. Moreover, they showed that at irrational distances a fractal structure of the diffraction field can be proved with sufficient experimental evidence.

Here, after briefly reviewing the results of Berry & Klein, we show that analogous results can be obtained easily for the case of dispersion in linear optical fibers. Moreover, we apply the wavelet transform [5] to the fractal Talbot problem. The point with the wavelet transform is that it contains more information with respect to the Fourier transform, which is behind the Helmholtz equation. Wavelet transforms have been considered as a very suitable mathematical microscope for fractals due to their ability to reveal the construction rules of fractals and to resolve local scaling properties as noticed before for the case of fractal aggregates [6].

2 Rational Talbot effect for Ronchi gratings

The diffraction due to Ronchi gratings can be approached analytically using the Helmholtz equation. Passing to dimensionless transverse and paraxial variables $\xi = x/a$ and $\zeta = z/a$, respectively, the scalar wave solution $\Psi(\xi, \zeta)$ of the Helmholtz equation can be expressed as a convolution in ξ of the Ronchi unit cell square function

$$g(\xi) = \left\{ \begin{array}{ll} 1 & \xi \in [-\frac{1}{4}, \frac{1}{4}] \\ 0 & \xi \ni [-\frac{1}{4}, \frac{1}{4}] \end{array} \right. , \tag{1}$$

and the Dirac comb transmittance, i.e.

$$\Psi(\xi, \zeta) = \int_{-1/2}^{+1/2} g(\xi') \left(\sum_{n=-\infty}^{\infty} \exp[i\, 2\pi n(\xi - \xi')] \exp[i\Theta_n(\zeta)] \right) d\xi' . \tag{2}$$

In the previous formulas, the unit cell is the single spatial period of the grating, which we take centered at the origin and of length equal to unity and $\Theta_n(\zeta) = 2\pi\zeta \frac{a^2}{\lambda^2} \sqrt{1 - \left(\frac{n\lambda}{a}\right)^2}$ is a phase produced by the diffraction of the Dirac comb 'diagonal' rays. The so-called Fresnel approximation for this phase is a Taylor expansion up to the second order for the square root leading to $\Theta_s(\zeta) \approx -\pi n^2 \zeta$. It can be easily shown now that in the Fresnel approximation Eq. 2 can be written as an infinite sum of phase exponentials in both variables ξ and ζ

$$\Psi_{\mathrm{p}}(\xi, \zeta) = \sum_{n=-\infty}^{\infty} g_n \exp[i\, 2\pi n\xi - i\pi n^2 \zeta] = \sum_{n=-\infty}^{\infty} g_n \psi_{\mathrm{p}}(\xi, \zeta) , \tag{3}$$

where the amplitudes g_n are the Fourier modes of the transmittance function of the Ronchi grating

$$g_n = \int_{-1/4}^{+1/4} \exp[-i\,2\pi n\xi']d\xi' \ . \tag{4}$$

Furthermore, by discretizing the optical propagation axis ζ by means of rational numbers, one can write the rational paraxial field as a shifted delta comb affected by phase factors, which is the main result of Berry and Klein:

$$\psi_{\mathrm{p}}\left(\xi, \frac{p}{q}\right) = \frac{1}{q^{1/2}} \sum_{n=-\infty}^{\infty} \Phi_{\mathrm{diffr}}(n; q, p)\,\delta\left(\xi_p - \frac{n}{q}\right), \tag{5}$$

where $\xi_p = \xi - e_p/2$ and $e_p = 0(1)$ if p is even (odd). The factors $\Phi_{\mathrm{diffr}}(n; q, p)$ are actually phase factors and will be specified in the next section. They appear to be the physical quantities directly connected to number theory. At the same time, this rational approximation allows for the following important physical interpretation of the paraxial self-imaging process: *in each unit cell of the plane p/q, q images of the grating slits are reproduced with spacing a/q and intensity reduced by $1/q$.*

3 Rational Talbot effect in linear optical fibers

As known, in fiber optics technology, electromagnetic dispersion is defined in terms of the *propagation constant* (wavenumber) of each frequency mode $\beta(\omega) = n(\omega)\frac{\omega}{c}$. In the following we will use one of the simplest optical fibers having a core-cladding step profile of the index of refraction. In addition, the famous slowly varying envelope approximation (henceforth SVEA) is a realistic approach when treating the propagation of quasi-monochromatic fields, such as laser fields and other types of coherent beams within such materials. For more details we refer the reader to textbooks [7].

SVEA means decomposing the electromagnetic fields in two factors: a rapidly varying phase component and a slowly varying amplitude field A enveloping the rapid oscillatory fields. The following Schrödinger-like dispersion equation can be obtained for A in the *SVEA* approximation

$$2i\frac{\partial A}{\partial z} = -\mathrm{sign}(\beta_2)\frac{\partial^2 A}{\partial \tilde{t}^2} \ , \tag{6}$$

where β_2 is the second coefficient in the Taylor expansion of the propagation constant in the neighbourhood of the central resonance frequency. This is the simplest form of the dispersion equation that one can envision in which actually no material propagation shows up. It can be fulfilled in the practical situation when the dielectric medium has sharp resonances ($\delta\omega_r \ll \omega_r$). Because of technological requirements, β_2 is usually a negative parameter corresponding to the so-called anomalous dispersion region. As can be seen, the SVEA equation has

exactly the same mathematical form as the diffraction equation in the paraxial approximation:

$$2i\frac{\partial\Psi_{\mathrm{p}}}{\partial z} = \frac{\partial^2\Psi_{\mathrm{p}}}{\partial x^2}\ ,\qquad(7)$$

where Ψ_{p} is the electric field close to the propagation axis.

Many results in diffraction can be translated to the case of dispersion in fibers by using the following substitutions

$$\begin{aligned} x &\rightarrow & \tilde{t} &\quad(\xi\rightarrow\tau)\\ y &\rightarrow & \mathbf{r} & \\ z &\rightarrow & z &\quad(\zeta\rightarrow\zeta). \end{aligned}$$

In the first row one passes from the grating axis to the time axis of a frame traveling at the group velocity of a pulse. In the second row one passes from the second grating axis that here we consider constant to the transverse section of the optical fiber. Finally, the propagation axis remains the same for the two settings. This *change of variables* will be used here to compare the results obtained in the two frameworks.

The general solution of the *SVEA* dispersion equation (6) for the amplitude $A(z,\tilde{t})$ depends on the initial conditions. Assuming a periodic input signal of period T written as a Fourier series, i.e., $A(0,\tilde{t}) = \sum_{n=-\infty}^{n=\infty} C_n^0 e^{-i\omega_n\tilde{t}}$, where C_n^0 are the Fourier coefficients of the initial pulse at the entrance of an optical fiber with linear response, one can write the pulse at an arbitrary z as follows:

$$A(z,\tilde{t}) = \sum C_n^0 \exp\left[i\frac{\omega_n^2 z}{2} - i\omega_n\tilde{t}\right]\qquad\text{where }\omega_n = 2\pi n/T.\qquad(8)$$

If the scaling of variables $\tau = \tilde{t}/T$, $\zeta = 2z/z_{\mathrm{T}}$ is employed, $A(z,\tilde{t})$ can be rewritten as

$$A(\zeta,\tau) = \sum C_n^0 \exp\left[i\pi n^2\zeta - i2\pi n\tau\right],\qquad(9)$$

because the Talbot distance corresponding to this case is $z_{\mathrm{T}} = T^2/\pi$. Just as in the context of diffraction, the convolution of the unitary cell with the propagator can be equally done before or after the paraxial approximation is employed. We notice that Eq. 9 can be also written as

$$A(\zeta,\tau) = \int_{-T/2}^{T/2} A(0,\tau')\alpha(\zeta,\tau'-\tau)d\tau'\qquad(10)$$

since C_n^0 are nothing but the Fourier coefficients of the input signal and where

$$\alpha(\zeta,\tau) = \sum_{n=-\infty}^{\infty} \exp\left[i\pi n^2\zeta - i2\pi n\tau\right]\qquad(11)$$

can be thought of as the analog of the paraxial propagator [4]. In this expression, the trick is to turn the continuous propagation axis into the rational number

4

axis and also to perform the integer modulo division of n with respect to the rational denominator of the propagation axis, i.e.,

$$\zeta = \frac{p}{q}, \qquad n = lq + s. \tag{12}$$

Through this approximation, the sum over n is divided into two sums: one over negative and positive integers l, and the other one over $s \equiv n \,(\mathrm{mod}\, q)$

$$\alpha\left(\frac{p}{q}, \tau\right) = \sum_{l=-\infty}^{\infty} \sum_{s=0}^{q-1} \exp\left[i\pi(lq+s)^2 \frac{p}{q} - i2\pi(lq+s)\tau\right]. \tag{13}$$

This form of $\alpha(\zeta, \tau)$ is almost exactly the same as given by Berry & Klein [4] and by Matsutani and Ônishi [8]. The difference is that the sign of the exponent is opposite. Following these authors one can express α in terms of the Poisson formula leading to

$$\alpha\left(\frac{p}{q}, \tau\right) = \frac{1}{\sqrt{q}} \sum_{n=-\infty}^{\infty} \left[\frac{1}{\sqrt{q}} \sum_{s=0}^{q-1} \exp\left[i\pi\left(\frac{p}{q}s^2 - 2s\tau\right)\right]\right] \delta\left(\tau_p + \frac{n}{q}\right), \tag{14}$$

where τ_p is a notation similar to ξ_p. We can also write Eq. 14 in the form

$$\alpha\left(\frac{p}{q}, \tau\right) = \frac{1}{\sqrt{q}} \sum_{n=-\infty}^{\infty} \Phi_{\mathrm{disp}}(n; q, p)\, \delta\left(\tau_p + \frac{n}{q}\right),$$

which is similar to Eq. 5. The rest of the calculations are straightforwardly performed though they are lengthy. By algebraic manipulations the phase factor can be easily obtained and we reproduce below the two expressions for direct comparison

$$\Phi_{\mathrm{disp}}(n; q, p) = \frac{1}{\sqrt{q}} \sum_{s=0}^{q-1} \exp\left\{i\frac{\pi}{q}\left[ps^2 - 2s(n - \frac{qe_p}{2})\right]\right\} \tag{15}$$

$$\Phi_{\mathrm{diffr}}(n; q, p) = \frac{1}{\sqrt{q}} \sum_{s=0}^{q-1} \exp\left\{i\frac{\pi}{q}\left[2s(n + \frac{qe_p}{2}) - ps^2\right]\right\}. \tag{16}$$

Both phases are special types of Gauss sums from the mathematical standpoint. The difference of signs here appears because of the sign convention chosen for the Fourier transform. Not surprisingly, the changes in the mathematical formulation are minimal although the experimental setup is quite different. The final results are the following:

p even, q odd:

$$\Phi_{\mathrm{disp}}(n; p, q) = \left(\frac{p}{q}\right)_J \exp\left(-i\frac{\pi}{4}\left[(q-1) + \frac{p}{q}(2n\bar{p}_q)^2\right]\right),$$

$$\Phi_{\mathrm{diffr}}(n; p, q) = \left(\frac{p}{q}\right)_J \exp\left(+i\frac{\pi}{4}\left[(q-1) + \frac{p}{q}(2n\bar{p}_q)^2\right]\right).$$

5

p odd, q odd:

$$\Phi_{\text{disp}}(n; p, q) = \left(\frac{p}{q}\right)_J \exp\left(-i\frac{\pi}{4}\left[(q-1) + 2\bar{2}_q^3\frac{p}{q}((2n-q)\bar{p}_q)^2\right]\right),$$

$$\Phi_{\text{diffr}}(n; p, q) = \left(\frac{p}{q}\right)_J \exp\left(+i\frac{\pi}{4}\left[(q-1) + 2\bar{2}_q^3\frac{p}{q}((2n+q)\bar{p}_q)^2\right]\right).$$

p odd, q even:

$$\Phi_{\text{disp}}(n; p, q) = \left(\frac{q}{p}\right)_J \exp\left(-i\frac{\pi}{4}\left[-p + \frac{p}{q}((2n-q)\bar{p}_q)^2\right]\right),$$

$$\Phi_{\text{diffr}}(n; p, q) = \left(\frac{q}{p}\right)_J \exp\left(+i\frac{\pi}{4}\left[-p + \frac{p}{q}((2n+q)\bar{p}_q)^2\right]\right).$$

In all these formulas, the so-called Jacobi symbols in number theory [9] lie in front of the exponentials and the bar notation defines the inverse in a given modulo class, i.e., $p\bar{p}_q \equiv 1 (\text{mod } q)$.

If one tries to make computer simulations using the Fourier transform method, the Gibbs phenomenon is unavoidable for discontinuous transmittance functions. However, in the case of fiber dispersion, one class of continuous pulses one could work with are the supergaussian ones, i.e., functions of the following form

$$A(\zeta = 0, \tau) = A_0 \exp\left[\frac{-\tau^N}{\sigma_0}\right], \tag{17}$$

where N is any even number bigger than two. The bigger the chosen N the more the supergaussian pulse resembles a square pulse. In our simulations we used the fixed value $N = 12$.

4 Irrational Talbot effect

4.1 Fractal approach

In the Talbot terminology the self-reconstructed images in the planes $z = (p/q)z_{\text{T}}$ consist of q superposed copies of the grating as already mentioned, completed with discontinuities. Although there is a finite number of images at fractional distances, they still represent an infinitesimal subset of all possible images that occur at the irrational distances.

In the planes located at irrational 'fractions' of the Talbot distance the light intensity is a *fractal function* of the transverse variable. The field intensity has a definite value at every point, but its derivative has no definite value. Such fractal functions are described by a fractal dimension, D, between one (corresponding to a smooth curve) and two (corresponding to a curve so irregular that it occupies a finite area). In the case of Ronchi gratings, for example, the fractal dimension of the diffracted intensity in the irrrational transverse planes is 3/2 [10].

To obtain the fractal Talbot images, Berry & Klein considered the irrational ζ_{irr} as the limit $m \to \infty$ of a sequence of rationals p_m/q_m. In particular, they employed the successive truncations of the continued fraction for ζ_{irr}, namely

$$\zeta_{\text{irr}} = a_0 + \frac{1}{a_1 + \left[\frac{1}{(a_2 + \cdots)}\right]} \ , \qquad (18)$$

where the a_m are positive integers. These sequences give best approximations, in the sense that p_m/q_m is closer to ζ_{irr} than any other fraction with denominator $q \leq q_m$. As a matter of fact, they considered the golden mean $\zeta_{\text{irr}} = (5^{1/2}-1)/2$, for which all a_m are unity, and the p_m and q_m are Fibonacci numbers. Because of the symmetries of the paraxial field, the Talbot images are the same at ζ_{G} and $\bar{\zeta}_{\text{G}} \equiv 1 - \zeta_{\text{G}}$, that is

$$\bar{\zeta}_{\text{G}} = \frac{3 - 5^{1/2}}{2} = 0.381966... = \lim_{\# \to \infty} \left\{0 \ , \ \frac{1}{2} \ , \ \frac{1}{3} \ , \ \frac{2}{5} \ , \ \frac{3}{8} \ , \ \frac{5}{13} \ , \ \frac{8}{21} \ , \ ...\right\} \ . \qquad (19)$$

Moreover, one can define the so-called *carpets* which are wave intensity patterns forming fractal surfaces on the (ξ, ζ) plane, i.e., the plane of the transverse periodic coordinate and the propagation coordinate. Since they are surfaces, their fractal dimension takes values between two and three. According to Berry, in general for a surface where all directions are equivalent, the fractal dimension of the surface is one unit greater than the dimension of an inclined curve that cuts through it. Taking into account that for a Talbot carpet the transverse image curves have fractal dimension $D = 3/2$, then the carpet's dimension is expected to be $5/2$. However, Talbot landscapes were found not to be isotropic. For fixed ξ, as the intensity varies as a function of distance ζ from the grating, the fractal dimension is found to be $7/4$, one quarter more than in the transverse case. Therefore the longitudinal fractals are slightly more irregular than the transverse ones. In addition, the intensity is more regular along the bisectrix canal because of the cancelation of large Fourier components that has fractal dimension of $5/4$. The landscape is dominated by the largest of these fractal dimensions (the longitudinal one), and so is a surface of fractal dimension $1+ 7/4 = 11/4$.

4.2   Wavelet approach

Wavelet transforms (WT) are known to have various advantages over the Fourier transform and in particular they can add up supplementary information on the fractal features of the signals [6]. The one-dimensional WT of f is defined as follows

$$W_f^h(\text{m}, \text{n}) = \int_{-\infty}^{\infty} f(\text{s})h_{\text{m},\text{n}}^*(\text{s})ds \qquad (20)$$

where $h_{\text{m},\text{n}}$ is a so-called daughter wavelet that is derived from the mother wavelet $h(\text{s})$ by dilation and shift operations quantified in terms of the dilation (m) and shift (n) parameters:

$$h_{\text{m},\text{n}}(\text{s}) = \frac{1}{\sqrt{\text{m}}} h\left(\frac{\text{s} - \text{n}}{\text{m}}\right) \qquad (21)$$

In the following, we shall use the Morlet wavelets which are derived from the typical Gaussian-enveloped mother wavelet which is itself a windowed Fourier transform

$$h(\text{s}) = \exp[-(\text{s}/\text{s}_0)^2]\exp(i2\pi k\text{s}). \tag{22}$$

The point is that if the mother wavelet contains a harmonic structure, e.g., in the Morlet case the phase $\exp(i2\pi k\text{s})$, the WT represents both frequency and spatial information of the signal.

In the wavelet framework one can write the expansion of an arbitrary signal $\varphi(t)$ in an orthonormal wavelet basis in the form

$$\varphi(t) = \sum_{\text{m}} \sum_{\text{n}} \varphi_{\text{n}}^{\text{m}} h_{\text{m,n}}(t) \; , \tag{23}$$

i.e., as an expansion in the dilation and translation indices, and the coefficients of the expansion are given by

$$\varphi_{\text{n}}^{\text{m}} = \int_{-\infty}^{\infty} \varphi(t) h_{\text{m,n}}(t) dt \; . \tag{24}$$

The orthonormal wavelet basis functions $W_{\text{m,n}}(t)$ fulfill the following dilation-translation property

$$h_{\text{m,n}}(t) = 2^{\text{m}/2} h(2^{\text{m}}t - \text{n}) \; . \tag{25}$$

In the wavelet approach the fractal character of a certain signal can be inferred from the behavior of its power spectrum $P(\omega)$, which is the Fourier transform of the autocovariance (also termed autocorrelation) function and in differential form $P(\omega)d\omega$ represents the contribution to the variance of a signal from frequencies between ω and $\omega + d\omega$. Indeed, it is known that for self-similar random processes the spectral behavior of the power spectrum is given by [11, 12]

$$P_{\varphi}(\omega) \sim |\omega|^{-\gamma_f} \; , \tag{26}$$

where γ_f is the spectral parameter of the wave signal. In addition, the variance of the wavelet coefficients possesses the following behavior [12]

$$\text{var}\,\varphi_{\text{n}}^{\text{m}} \approx (2^{\text{m}})^{-\gamma_f} \; . \tag{27}$$

These formulas are certainly suitable for the Talbot transverse fractals because of the interpretation in terms of the regular superposition of identical and equally spaced grating images. We have used these wavelet formulas in our calculations related to the same rational paraxiallity for the two cases of transverse diffraction fields (Fig. 1) and the fiber-dispersed optical fields (Fig. 2), respectively. The basic idea is that the above-mentioned formulas can be employed as a checking test of the self-similarity structure of the optical fields. The requirement is to have a constant spectral parameter γ_f over many scales. In the case of supergaussian pulses, their dispersed fields turned out not to have the self-similarity property as can be seen by examining Fig. 2 where one can see that the constant slope is not maintained over all scales. In Figs. 3 and 4

the behavior of the wavelet transform using Morlet wavelets for the diffraction field is displayed. A great deal of details can be seen in all basic quantities of the diffracted field, namely in the intensity, modulus, and phase. On the other hand, the same wavelet transform applied to the N=12 supergaussian dispersed pulse (see Fig. 5), although showing a certain similarity to the previous discontinuous case, contains less structure and thus looks more regular. This points to the fact that if in diffraction experiments one uses continuous transmittance gratings the fractal behavior would turn milder.

5   Conclusion

The fractal aspects of the paraxial wavefield have been probed here by means of the wavelet transform for the cases of diffraction and fiber dispersion. In the case of diffraction, the previous results of Berry and Klein are confirmed showing that the wavelet approach can be an equivalent and more informative tool. The same procedure applied to the case of fiber dispersion affecting the paraxial evolution of supergaussian pulses indicates that the self-similar fractal character does not show up in the latter type of axial propagation. This is a consequence of the continuous transmittance function of the supergaussian pulses as opposed to the singular one in the case of Ronchi gratings.

As a promising perspective, we would like to suggest the following experiment by which irrational distances can be determined. The idea is that the spectral index of the Talbot fractal images can be used as a very precise pointer of rational and irrational distances with respect to the Talbot one. Suppose that behind a Ronchi grating under plane wave illumination a CCD camera is mounted axially by means of a precision screw. The Talbot image at $z_{\rm T}$ can be focused experimentally and can be used to calibrate the whole system. An implemented real time wavelet computer software can perform a rapid determination of the fractal index γ_f, which in turn allows the detection of changes of the distance in order to determine if the CCD camera is at rational or irrational multiples of the Talbot distance. Supplementary information on the irrational distances may be obtained from the amplitude-phase wavelet representations. To the best of our knowledge, we are not aware of another experimental setup in which irrational distances can be determined in such an accurate way. This also points to high-precision applications in metrology.

Finally, we mention that a version of this work with more mathematical details will appear soon [13].

6   Acknowledgements

References

[1] H.F. Talbot, Phil. Mag. **9**, 401-407 (1836).

[2] Lord Rayleigh, Phil. Mag. **11**, 196-205 (1881).

[3] K. Patorski, Prog. Opt. XXVII, 1-108 (1989).

[4] M.V. Berry and S. Klein, J. Mod. Opt. **43**, 2139-2164 (1996); See also: J.T. Winthrop and C.R. Worthington, J. Opt. Soc. Am. **49**, 373-381 (1965); O. Bryngdahl, *ibidem* **63**, 416-419 (1973).

[5] J.S. Walker, *A Primer on Wavelets and their Scientific Applications* (Chapman & Hall, CRC Press, 1999).

[6] A. Arneodo, G. Grasseau, M. Holschneider, Phys. Rev. Lett. **61**, 2281 (1988); E. Freysz *et al*, Phys. Rev. Lett. **64**, 745 (1990); F. Argoul *et al*, Phys. Rev. **A41**, 5537 (1990).

[7] G.P. Agrawal, *Nonlinear Fiber Optics* (Second Ed., Academic Press, 1995).

[8] S. Matsutani and Y. Ônishi, Found. Phys. Lett. **16**, 325 (2003), math-ph/0207011.

[9] N. Koblitz, *A Course in Number Theory and Cryptography* (2nd Ed. Springer Verlag, 1994).

[10] M. Berry, I. Marzoli, and W. Schleich, Phys. World, 33-44 (June 2001).

[11] G.W. Wornell and A.V. Oppenheim, IEEE Trans. Inform. Theory **38**, 785-800 (1992).

[12] W.J. Staszewski and K. Worden, Int. J. Bif. Chaos **3**, 455 (1999).

[13] H.C. Rosu *et al*, Int. J. Mod. Phys. B (2006).

First Four Figure Captions

Fig. 1: (a) The fractal Talbot light intensity $|\Psi_{\mathrm{p}}|^2$ at the twelfth Fibonacci fraction $\zeta = 144/377 \approx 0.381963$, which is already 'very close' to $\bar{\zeta}_{\mathrm{G}}$ and (b) the plot of the logarithmic variance of its wavelet coefficients (Eq. 24). The line of negative slope of the latter semilog plot indicates fractal behavior of the diffraction wavefield as we expected. The fractal coefficient is given by the slope and its calculted value is γ_f.

Fig. 2: Snapshot of the dispersed supergaussian pulse for $N = 12$ at $\zeta = 144/377$. The log variance plot is monotonically decreasing displaying a plateau indicating a nonfractal behaviour of the $N = 12$ supergaussian pulse train.

Fig. 3: The wavelet transform of the intensity $|\Psi_{\mathrm{p}}|^2$ at fixed $\zeta = 144/377$ for (a) the unit cell and (b) half-period displaced grating unit cell. There is no difference because the square modulus is plotted.

Fig. 4: Wavelet representations of: (a) the squared modulus of the amplitude and (b) phase of the Talbot diffraction field for fixed $\zeta = 144/377$ and a displaced unit cell.
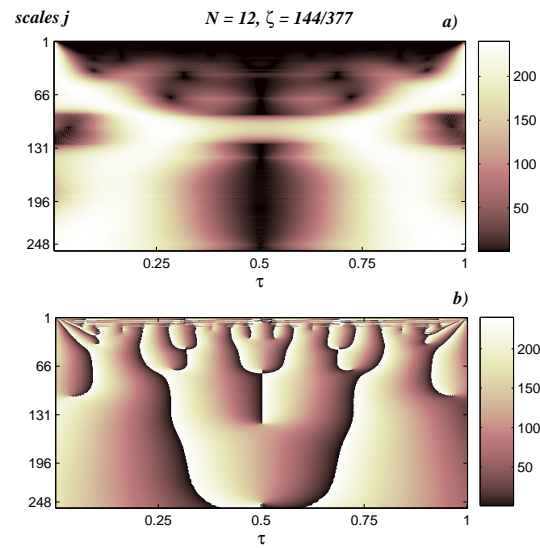
Figure 1: (Color online) Wavelet representations of the (a) amplitude and (b) phase of the Talbot dispersed supergaussian field ($N = 12$) for $\zeta = 144/377$.